Sequential Detection for Passive Radar Part 1: The A-C DF-map Detector

Tri-Tan Van Cao
Defence Science & Technology (DST) Group
Building 180, DST Group Edinburgh
Adelaide, Australia
tan.cao@dst.defence.gov.au

***Abstract*—Design of constant false alarm rate (CFAR) detectors for a multi-channel passive coherent location (PCL) radar system is addressed in this paper. Two sequential detectors with alert-confirm (A-C) mechanism are proposed: the A-C direction finding (DF) map detector and the A-C Guard detector. This Part 1 is devoted to the A-C DF-map detector, while the A-C Guard detector is presented in the companion paper Part 2. The A-C DF-map detector operates on the DF-map only in its alert step, whereas its confirm step is performed in the direction of the suspected target's angle-of-arrival. Monte-Carlo analysis shows that the sequential detector has outstanding detection gain compared to the case of the conventional one-step detector, while testing with experimental data shows significant improvement in detection performance.**

Keywords—CFAR; Sequential alert-confirm detection; passive coherent location radar.

I. INTRODUCTION

For target detection, passive coherent location (PCL) radar employs illuminating sources which are available in the environment such as FM radio, VHF/UHF digital terrestrial television broadcasting signals instead of using its own transmission as in the case of an active radar. PCL radar is therefore potentially undetectable, difficult to jam, low-cost to build, and inexpensive to operate since an electro-magnetic transmission license is not required [1].

While it takes an active radar a number of coherent processing intervals (CPIs) to completely scan through the whole surveillance space to detect targets, a multi-channel PCL radar is capable of performing such surveillance task within every single CPI. The reason is that PCL radar can take advantage of a surveillance space which is illuminated by the broadcasting sources at all times. In principle, such capability can be realized by forming many receive beams during each CPI to cover the whole surveillance space and checking for target presence/absence in each cell of a range-Doppler (RD) map obtained at each beam. The computation required for beamforming and detection processing in a PCL radar is, therefore, many times heavier than that of an active radar. Such huge signal processing and detection load would hinder the real-time capability of a multi-channel PCL system.

In order to give real-time capability, several beamforming and detection schemes have been proposed in the open literature, each of them has its own advantage and drawback regarding the balance between real-time capability and detection loss. The aim of this paper is to design a detection scheme for a multi-channel PCL system, which is real-time capable while minimising the detection loss.

The signal processing and target detection of a multi-channel PCL system are summarized as follows. Firstly, RD processing is carried out by correlating the reference signal (known as the line-of-sight (LOS) channel) with the signal received at each antenna element (known as the surveillance channel), and then by performing a fast Fourier transform (FFT) on the range correlation results. Secondly, using the RD processing results from all antenna elements, receive beams are formed covering all resolution angles in the surveillance space to generate directional RD-maps [2]. In principle, each cell in each directional RD-map should be checked for target presence using a sliding window (SW) constant false alarm rate (CFAR) detector [3]. However, performing CFAR detection in this way requires the computation and storage of the sample and the interference estimate in every range/Doppler/Angle-of-arrival (AoA) bin. This can hardly be done in real-time [2,4].

In order to give real-time capability, a signal processing technique based on a direction finding (DF) map is proposed in [2]. For each RD-map cell, n_A beams are formed (steering at n_A resolution angles in the surveillance space) and the beam direction in which the beamforming response is the highest is hypothesised as the AoA of the target. The signal strength at the hypothesised AoA is kept to form the so-called DF-map. In this way, the 3-dimensional (3D) data cube is transformed into a single 2D map (the DF-map). Target detection can then be performed in real-time by applying a CFAR detector on the DF-map, and the target's AoA can be deduced since each DF-map cell corresponds to one hypothesised target's AoA. However, performing CFAR detection on the DF-map would lead to severe detection loss. In the DF-map, the target's signal-to-noise ratio (SNR) is the ratio between the signal strength in the cell-under-test (CUT) and the interference level estimated as the mean of a set of reference cells surrounding the CUT. Those reference cells are contaminated in the formation of the DF-map, since each of them is the highest noise/clutter return from all AoAs. Those contaminated reference cells contain more energy than the background noise, leading to reduced target SNR.

Another detection scheme which strikes a balance between detection performance and real-time capability is proposed in

[4]. In this technique, two sets of beams are employed for beamforming which is carried out in two stages. In the first stage, the search space is divided into n_1 subsectors and a set of n_1 beams is formed (each beam has a large beamwidth which covers one subsector). This generates n_1 RD-maps which are then used for CFAR detection. In the second stage, the AoA of each target declared in the first stage is determined by a direction finding procedure which uses a set of n_2 beams (each having a much finer beamwidth) to cover the sub-sector which contains the declared target. As will be elaborated later, one disadvantage of this two-stage beamformer technique is that it has a few dB of CFAR loss compared with the performance of the optimal detector.

In the two-stage beamformer technique [4], target presence/absence decision is made in only one step, in the sense that only one threshold test is performed for each decision. There are two approaches to radar detection. In the first approach known as one-step detector, the target presence/absence decision is made after a fixed interval of observation, for instance, after collecting the data in one CPI. In the second approach known as sequential detection, the interval of observation is not fixed but varies depending on the observation results [5]. A typical sequential detection implementation is the two-step alert-confirm (A-C) detector. For active radars which use their own transmission, sequential A-C detectors can give an improvement of more than 4 dB in detection sensitivity compared to one-step detectors [6] p70.

In each CPI, millions of cells are to be examined to search for only a few targets. Practically, certain cells deserve more examination effort than the others do. The A-C structure of a sequential detector provides a mechanism to realise such examination strategy in order to save time and radar resources.

Two sequential CFAR detectors, namely the A-C DF-map detector and the A-C Guard detector are proposed. This paper is Part 1 which is devoted to the A-C DF-map detector, while the A-C Guard detector is presented in the companion paper Part 2 [7]. The paper is organised as follows. The new A-C DF-map detection scheme and its signal processing load are presented in Sections II and III. Method of probability estimation is explained in Section IV, followed by the analysis of false alarm and detection performances in Sections V and VI, respectively. The proposed detector is then tested on a real target scenario and compared with the two-stage beamformer technique in Sections VII and VIII, respectively.

II. The A-C DF-Map Detection Scheme

The A-C DF-map detector for an M-channel PCL radar is proposed as in Fig. 1 (right). After the formation of M elementary RD-maps at M channels, a target presence/absence decision is made in two steps.

Alert: the DF-map is formed and each of its cells is checked for the suspicion of a target. Let x be the signal strength in the CUT. L_1 cells around the CUT are selected to form the set of reference cells $\{x_1,\ldots,x_{L1}\}$. A number of gap cells in the immediate neighbourhood of the CUT are excluded. A target suspicion is declared at the CUT if the following cell-averaging (CA) threshold test is passed:

$$x > T_1\mu_1 \tag{1}$$

Otherwise, target absence is declared. In (1), T_1 is a constant whose value is determined by the alert false alarm rate F_1; and μ_1 is the interference estimate which is the mean of L_1 reference cells. Since each DF-map cell corresponds to one hypothesized AoA, the suspected target's AoA is the hypothesized AoA of the CUT.

Confirm: each DF-map cell that passes the alert test is checked for target presence/absence as follows. Perform beamforming in the hypothesised target's AoA to obtain L_2 reference cells $\{z_1,\ldots,z_{L2}\}$ in the range-Doppler neighbourhood of the CUT. A target is declared present at the (suspected) CUT if:

$$x > T_2\mu_2 \tag{2}$$

Otherwise, target absence is declared. In (2), x is the sample in the CUT; μ_2 is the interference estimate which is the mean of the L_2 reference cells; and T_2 is a constant determined by the combined alert-confirm false alarm rate F.

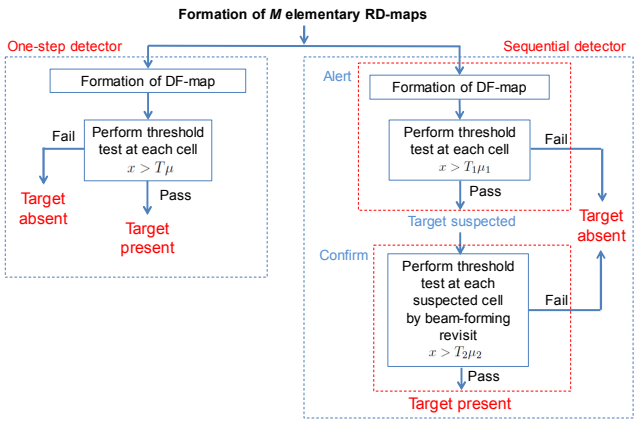

Fig. 1 Sequential A-C DF-map detector versus one-step detector.

Remark: For the sequential detection technique discussed in the open literature (see [5], for instance), after the alert test is passed in the current CPI, the confirm test is then performed in the next CPI. In this paper, for simplicity, the same CPI is used for both tests (1) and (2). Test (2) helps to avoid the reference cell contamination problem encountered in test (1) (due to the formation of the DF-map).

III. Signal Processing Load

The signal processing and detection loads of the A-C DF-map detector are now compared to those of the conventional one-step detector. The one-step detector operates as in Fig. 1 (left). After the formation of M elementary RD-maps at M channels, the DF-map is formed and each of its cells is checked for target presence/absence. A target is declared present at a CUT x if the following test is passed:

$$x > T\mu \tag{3}$$

Otherwise, target absence is declared. In (3), T is a constant whose value is determined by the false alarm rate F; and μ is the mean of L reference cells (selected from the DF-map).

For the one-step detector, a data cube consisting of $S_1 = KN$ samples is required to form the DF-map, where K is the number of surveillance angles in the surveillance space and N is the number of cells in the DF-map. For the A-C DF-map detector, the alert step data cube is S_1 (the same as that for the one-step detector). The number of DF-map cells that survive the alert step is NF_1, where F_1 is the alert false alarm rate. Since L_2 reference samples are required in order to perform a confirm threshold test on each of those NF_1 cells, the total data samples generated in the confirm step is $S_2 = NF_1L_2$. The signal processing load ratio A-C-DF-map-detector to one-step-detector is then $\rho_1 = (S_1+S_2)/S_1 = 1+(F_1L_2/K)$.

The number of threshold tests performed by the one-step detector is N (i.e. the number of cells in the DF-map), while that performed by the A-C DF-map detector is $N+NF_1=N(1+F_1)$ (i.e. N tests in the alert step and NF_1 tests in the confirm step). The ratio of number of threshold tests, A-C DF-map to one-step, is then $\rho_2=N(1+F_1)/N=1+F_1$. Given typical values $F_1=0.05$, $L_2=40$ reference samples, and $K=300$ surveillance angles, then $\rho_1 \approx 1.007$ and $\rho_2=1.05$. In summary, the two detectors have approximately the same signal processing and detection load. Therefore, if the one-step detector is real-time executable, then the A-C DF-map detector should also be real-time executable.

IV. Method of Probability Estimation

Due to the difficulty in obtaining closed-form formulas, the false alarm probability and detection probability of the one-step detector and the AC DF-map detector are estimated via Monte-Carlo simulation using experimental data. Each value of the false alarm probability is estimated by running a CA sliding-window detector over the homogeneous region of an experimental DF-map. Approximately 10^6 Monte-Carlo trials are performed to obtain the estimate of one false alarm probability value, while each value of the detection probability is estimated by inserting simulated targets with 10^4 Monte-Carlo trials. For the experimental data in use, the receiver parameters are summarised in Table 1, while the transmitter is a Digital Video Broadcast - Terrestrial (DVB-T) with carrier frequency 184.5 MHz and 7 MHz bandwidth.

TABLE I. Summary of Receiver Parameters

Surveillance Elements	**7**
Reference Elements	1
Surveillance Array Configuration	Ring
Surveillance Type	Dipole
Coherence Processing Interval	0.5 s
Frequency Band	171 – 220 MHz

Although not shown here, it is found that only the background interference of the squared-law RD-map obtained by beamforming in each individual AoA in the surveillance space has exponential distribution, while that of the (squared-law) DF-map does not. The non-Rayleigh characteristic of the DF-map is due to the peak selection operator performed on the AoA profile at each range-Doppler location. It is well-known in radar detection that the CA detector only has a CFAR characteristic if the background interference is exponentially distributed [8]. Therefore, it is anticipated that the one-step detector is not CFAR, and that only the confirm step of the sequential detector is CFAR.

V. Probability of False Alarm

A. One-step Detector

From (3), the false alarm probability of the one-step detector performed on the DF-map is:

$$F_{DF}=\text{Prob}[x > T\mu \mid H_0] \tag{4}$$

where H_0 is the hypothesis of target absence. In this section, given the number of reference cells L and the required false alarm rate F_{DF}, an approximation formula for computing the threshold multiplier T of the one-step detector is derived.

Consider the case $L = 40$. A data set consisting of 100 DF-maps is employed to estimate the false alarm rate of the one-step detector, giving 100 false alarm curves as shown in Fig. 2 (left). The average of those 100 curves is shown in Fig. 2 (right). It is evident that the CA sliding-window detector does not give the CFAR characteristic. For instance, the threshold multiplier $T=9.5$ gives an average false alarm of 10^{-4} as read from Fig. 2 (right). This value of threshold multiplier $T=9.5$ gives a false alarm fluctuation between $10^{-3.6}$ and $10^{-4.5}$ as seen in Fig. 2 (left), which means the fluctuation is 3 times of the nominal value 10^{-4}. For the CA-CFAR detector applied on exponential background, the threshold multiplier T can be computed in closed-form by [8]:

$$T=f(F,L)=[F^{-(1/L)}-1]\,L \tag{5}$$

where F is the CA-CFAR false alarm rate. It is found that the average curve can be approximated as:

$$T=f(3F_{DF},L) \tag{6}$$

where the function f is given in (5). This approximation gives the dash-dot curve in Fig. 2 (right).

Consider the case L is within [16,60]. By repeating the above procedure, it is found that the threshold multiplier T of the one-step detector can also be approximated using (6).

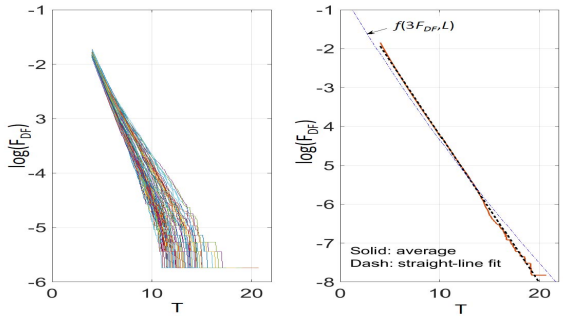

Fig. 2 False alarm curves of the one-step detector obtained by applying a CA sliding-window detector (with 40 reference cells) on the DF-map.

B. A-C DF-map Detector

From (1) and (2), the A-C DF-map detector has four parameters to be designed: (F_1,L_1) and (F,L_2). For simplicity, let $L_1=L_2=L$. Typically, the overall false alarm rate is $F = 10^{-6}$. In this section, assume that F_1 and F have been selected, approximation formulas for computing the threshold multipliers T_1 and T_2 are derived for L within [16,60].

As the alert step performs CA detector on the DF-map as in the case of the one-step detector, T_1 can be computed using (6):

$$T_1=[(3F_1)^{-(1/L)}-1]L \quad (7)$$

The overall false alarm rate is:

$$F=\text{Prob}[x>T_1\mu_1 \mid \text{H}_0]\times\text{Prob}[x>T_2\mu_2 \mid \text{H}_0]|_{\text{alert}}=F_1\times F_2 \quad (8)$$

where "$|_{\text{alert}}$" denotes a probability conditioned on the event that the alert test has been passed. This conditional probability means that the order of the tests, (1) followed by (2), is important. Such sequential detection strategy is different from the two-stage detectors presented in [9] in which the order of the two detection stages is not significant.

Consider the case L=40 and F_1=0.01. T_1 is computed as in (7). Using the same data set as in Section V.*A*, the false alarm F in (8) is estimated over an interval of T_2, giving 100 false alarm curves as shown in Fig. 3 (left). The average of those 100 curves is shown in Fig. 3 (right). It is observed that the sequential detector is not CFAR. For instance, the threshold multiplier T_2=11 gives an average false alarm of 10^{-4} as read from Fig. 3 (right). This value of T_2 gives a false alarm rate fluctuation between $10^{-3.8}$ and $10^{-4.2}$ as seen in Fig. 3 (left). That means the fluctuation is 1.6 times the nominal value 10^{-4}.

Consider the case L=40 and F_1 is within $[10^{-3},10^{-1}]$. The average overall false alarm curves are shown in Fig. 4 (left). It is observed that those false alarm curves converge to one curve for F_1 higher than 10^{-2}. A straight-line fit on the section between the two points A and B (corresponding to false alarm rates between 10^{-3} and 10^{-2}) is shown in Fig. 4 (right), dash line. Note that the confirm step is the CA-CFAR detector applied on exponential background: its false alarm curve is then given by (5). In Fig.4 (right), the false alarm curve for which T_2 is computed using (5) is shown with a solid line, that means:

$$T_2=[F^{-(1/L)}-1]\,L \quad (9)$$

It is observed that for values of false alarm rates F of practical interest between 10^{-7} and 10^{-5}, those two curves are very close together. For this reason, (9) is used for approximating the threshold multiplier T_2 of the confirm step given the overall false alarm F.

It is found that T_2 can also be approximated using (9) for the case L within [16,60] and F_1 within $[10^{-2},10^{-1}]$.

VI. Probability of Detection

The probability of detection (P_d) of the one-step and the A-C DF-map detectors are estimated using (4) and (8) respectively, by replacing hypothesis H_0 (target absence) with hypothesis H_1 (target presence). Swerling-1 targets [8] are inserted into the experimental data employed in Section V. For detection comparison the figure of merit CFAR loss is used, which is the additional target's signal-to-noise ratio (SNR) required for a detector to achieve the same detection probability as that of the CA-CFAR detector operating on exponential distribution (optimal performance). SNR of the inserted target is the SNR obtained after beamforming in the target's AoA. Based on detection performance, selection of the alert false alarm rate of the A-C DF-map detector is also examined.

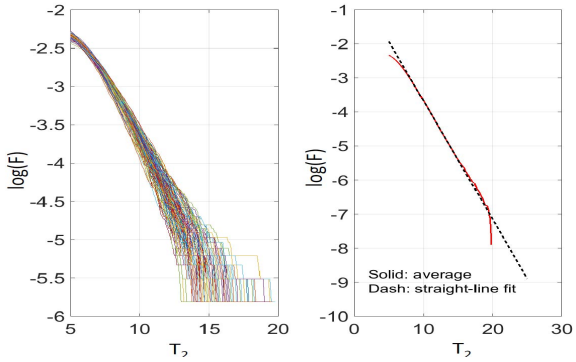

Fig. 3 False alarm curves of the A-C DF-map detector obtained using a CA sliding-window detector. Case L=40 and F_1=0.01.

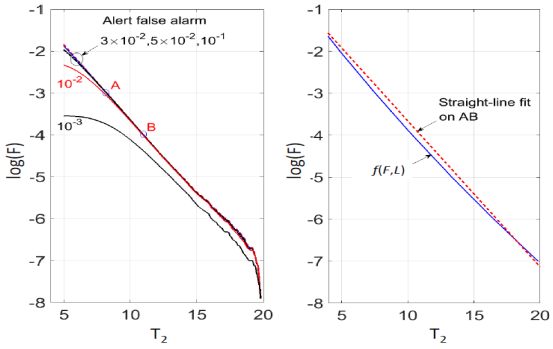

Fig. 4 False alarm curves of the A-C DF-map detector obtained using a CA sliding-window detector. Case L=40 and F_1 within $[10^{-3},10^{-1}]$.

Parameters of the two detectors are set as follows: one-step detector: F=10^{-6}, L=40; A-C DF-map detector: F=10^{-6}, L=40, F_1=3×10^{-2}. Assume that a target's AoA is randomly distributed over the whole 360° surveillance space. Detection probability for those two detectors is shown in Fig. 5 (top). The P_d curves of the optimal and A-C DF-map detectors almost superimpose on each other, while that of the one-step detector has approximately 5 dB CFAR loss. The receiver operating characteristic (ROC) curves for a target with 15 dB SNR are shown in Fig. 5 (bottom). For the overall false alarm within $[10^{-6},10^{-5}]$, the P_d of the sequential detector is very close to that of the optimal curve while the one-step detection is 35 % below. In Fig. 6, the P_d curves of the A-C DF-map detector are shown for different values of F_1. The A-C DF-map performance is closer to the optimal curve "Opt" with higher values of F_1. A reasonable choice is F_1 within $[10^{-2},10^{-1}]$, limiting the CFAR loss to less than 2 dB.

VII. Experimental Results

Performance of the proposed A-C DF-map detector is now tested using data collected by a PCL radar built by the Defence Science & Technology (DST) Group. The receiver has a 7-element ring array and a dedicated reference antenna for LOS signal reception. A total of 300 azimuth-elevation hypotheses are considered, covering 360^{O} azimuth and two layers of elevation. The reference signal is received from a DVB-T source with carrier frequency 184.5 MHz and a 7 MHz bandwidth. Receiver parameters are summarised in Table 1.

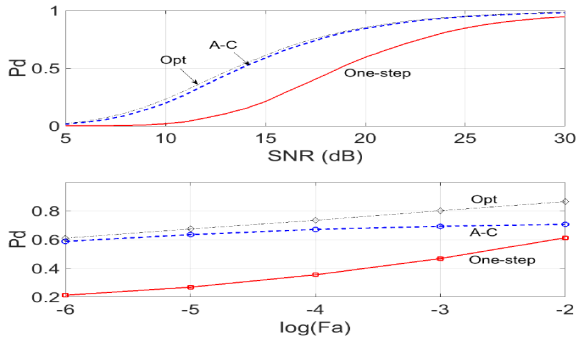

Fig. 5 Detection probability of the sequential detector.

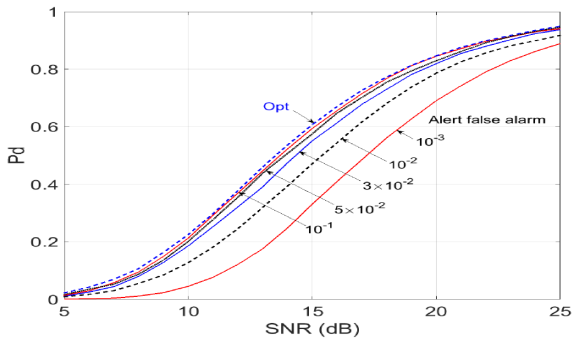

Fig. 6 Detection probability of the sequential detector at an overall false alarm rate of 10^{-6} with different alert false alarm rates.

Target ground truth scenario is shown in Fig. 7. The receiver is located at the origin (0,0) and is marked as Rx, while the transmitter is south-east of the receiver and is marked as Tx (164^{O} clock-wise from the true north). There is one Boeing 717 aircraft (labelled as B717); three Diamond D40 aircraft DA40(1), DA40(2), and DA40(3); one Diamond D42 aircraft labelled as DA42; and one Fokker F100 labelled as F100. The ground truth of those targets is shown as circles with arrows indicating their heading directions.

Parameters of the two detectors are: one-step (F = 10^{-6}, L=40); A-C DF-map: (F = 10^{-6}, L=40, F_1 = 10^{-2}). For both detectors, 5 gap cells on each side of the CUT are used. The data set is processed with a CPI length of 0.5 seconds, giving a total of 44 CPIs.

Target detection versus ground truth for B717 and DA40(2) is presented in Fig. 8. Target ground truth is marked with plus signs while target detection is marked with rectangular dots. As evident in Fig. 8 (bottom-right), the one-step detector gives only two detection points for target DA40(2); while in Fig. 8 (top-right), a more complete detection history of this target is given by the sequential detector. Target detection versus ground truth for DA40(1) and DA40(3) is presented in Fig. 9. The one-step detector misses the whole history of those two targets (Fig. 9, bottom-left, bottom-right); whereas the sequential detector gives many detection points which match with target ground truth (Fig. 9, top-left, top-right).

As evident in Fig. 8 and Fig. 9, it is apparent that the sequential detector gives reasonable false alarm performance in the confirm step, in the sense that the small neighbourhoods of the target ground truth are almost free of detection points which appear to be random, compared with detections that align in lines of correlated points along the target ground truth. In addition, it is found that the false alarm rate F_1 reported in the alert step is approximately 80 % of the nominal value.

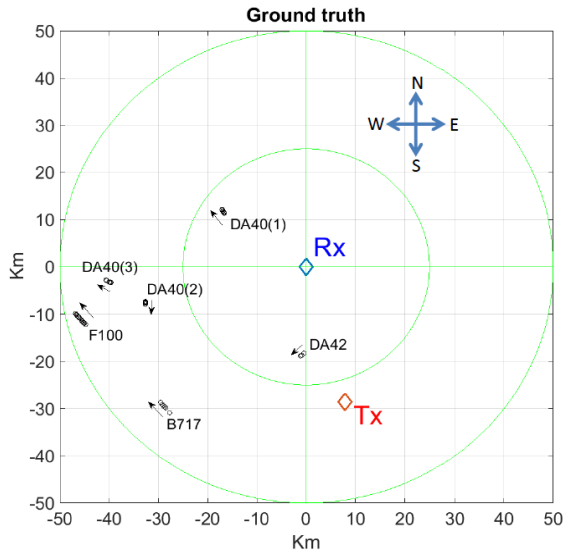

Fig. 7 The ground truth of target scenario. Rx: receiver; Tx: transmitter.

VIII. Discussion

The proposed sequential detector is compared with the two-stage beamformer technique [4] in this section. The two-stage beamformer technique is summarised as follows. Two sets of beams are employed for beamforming which is carried out in two stages. In the first stage, a set of 11 beams is employed to cover a search sector of 90^{o} (each beam has an azimuth resolution of 9^{o}). This generates 11 RD-maps which are then used for CFAR detection. In the second stage, the AoAs of targets declared in each of those 11 sub-sectors are determined by a direction finding procedure which uses a set of 9 beams (each has resolution of approximately 1^{o}) to cover the sub-sector under consideration.

The advantage of this two-stage beamforming technique is that it is real-time executable as presented in [4]. It can distinguish two targets which share the same bistatic range-Doppler location but coming from two different azimuth angles, provided that those two angles are at least 9^{o} apart. It

also has CFAR characteristic (whereas the false alarm rate of the A-C DF-map detector fluctuates 1.6 times around the nominal value 10^{-4}).

The disadvantage of the two-stage beamforming technique is explained as follows. To cover the full 360° surveillance as in the case of the sequential detector, 44 RD-maps corresponding to 44 sub-sectors are to be generated. To account for two layers of elevation coverage, then a total of 88 RD-maps are to be generated. Assume that each RD-map has 1 million cells, then the two-stage beamformer makes 88 million decisions on target presence/absence per CPI, while the sequential detector makes just over 1 million decisions per CPI. This means that, on the one hand, the detection load of the two-stage beamformer is 88 times that of the sequential detector. On the other hand, as the sequential detector only makes 1 million decisions (on target presence/absence) per CPI, a false alarm rate of 10^{-6} (as set in Section VII) gives approximately 1 false alarm per CPI. Since the two-stage beamformer makes 88 million decisions, its false alarm rate should be set at $1/(88\times10^{6}) \approx 10^{-8}$ in order to give the same number of false alarms of approximately 1 per CPI. Assume CA-CFAR detection on exponential background, detection at a false alarm rate of 10^{-8} has a detection loss of around 1.5 dB compared with detection at a false alarm rate 10^{-6}. This means that the two-stage beamforming technique has a CFAR loss around 1.5 dB compared with the sequential detector.

IX. Conclusion

A new sequential detector is proposed for target detection in the full 360° surveillance space of a multi-channel PCL system. The detection performance is analysed via Monte-Carlo simulation using experimental data, while a real detection scenario is employed to verify its performance. Closed-form formulas are derived for approximating the sequential detection threshold multipliers given the required false alarm rates. Monte-Carlo simulation shows that the false alarm rate of the sequential detector fluctuates within a small margin around the nominal value. Experimental results from a real target scenario show that the sequential detector has a detection performance which outperforms that of the conventional one-step detector.

Acknowledgement

All experimental data files analysed in this paper were obtained thanks to the support of the DST Group's PCL team. The readability of the paper is improved thanks to inputs from Mr Robert Young and Dr Brett Haywood.

References

[1] W.L. Melvin and J.A. Caheer, Principles of Modern Radar: Advanced Techniques, Chapter 17, SciTech Publishing, 2014, USA.

[2] J. Palmer, "A signal processing scheme for a multichannel passive radar system", ICASSP 2015, Brisbane, pp. 5575-5579.

[3] G. Weinberg, Radar Detection Theory of Sliding Window Processes, Taylor & Francis, CRC Press 2017.

[4] G. Bournaka, J. Heckenbach, A. Baruzzi, D. Cristallini and H. Kuschel, "A two-stage beamforming approach for low complexity CFAR detection and localisation for passive radar", IEEE Radar Conference 2016.

[5] J.V. DiFranco and W.L. Rubin, Radar Detection, Artech House 1980.

[6] D.K. Barton, Radar System Analysis and Modeling, Artech House 2005.

[7] T.V. Cao, "Sequential detection for passive radar, Part 2: the A-C Guard detector", IEEE Radar Conference 2018, Brisbane, Australia.

[8] P.P. Gandhi and S.A. Kassam, "Analysis of CFAR processors in nonhomogeneous background", IEEE Transactions on Aerospace & Electronic Systems, 1988, 24, (4), pp427-445.

[9] A. De Maio (Editor), Modern Radar Detection Theory, Chapter 4, Scitech Publishing, 2016.

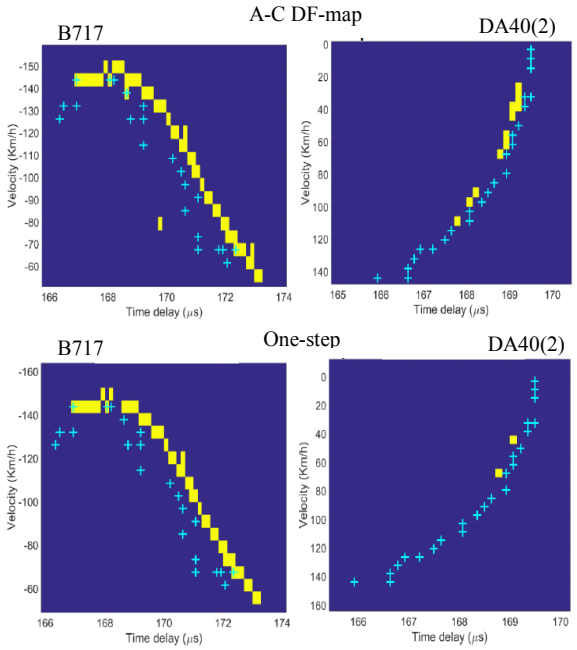

Fig. 8 Detection of targets B171 and DA40(2) versus ground truth. Rectangular dots: detections; plus signs: ground truth.

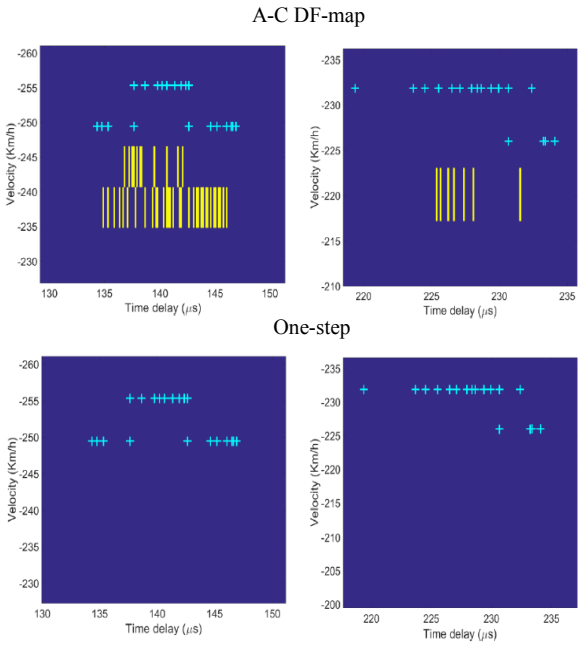

Fig. 9 Detection of targets DA40(1) and DA40(3) versus ground truth. Rectangular dots: detections; plus signs: ground truth.